ACS APPLIED MATERIALS & INTERFACES

Research Article

Cite This: ACS Appl. Mater. Interfaces 2020, 12, 963−969

www.acsami.org

Adapting Aluminum-Doped Zinc Oxide for Electrically Conductive Membranes Fabricated by Atomic Layer Deposition

Wulin Yang,[†] Moon Son,[†] Ruggero Rossi,[†] Johannes S. Vrouwenvelder,[‡] and Bruce E. Logan*[,†]

[†]Department of Civil and Environmental Engineering, The Pennsylvania State University, University Park, Pennsylvania 16802, United States

[‡]Water Desalination and Reuse Center (WDRC), Division of Biological and Environmental Science and Engineering (BESE), King Abdullah University of Science and Technology (KAUST), Thuwal 23955-6900, Saudi Arabia

Supporting Information

ABSTRACT: The use of electrically conductive membranes has recently drawn great interest in water treatment as an approach to reduce biofouling. Most conductive membranes are made by binding nanoparticles (carbon nanotubes or graphene) to a polymeric membrane using additional polymers, but this method risks leaching these nanomaterials into the environment. A new approach was developed here based on producing an electrically conductive layer of aluminum-doped zinc oxide (AZO) by atomic layer deposition. The aqueous instability of AZO, which is a critical challenge for water applications, was solved by capping the AZO layer with an ultrathin (∼11 nm) TiO_2 layer (AZO/TiO_2). The combined film exhibited prolonged stability in water and had a low sheet resistance of 67 Ω/sq with a 120 nm-thick coating, while the noncapped AZO coating quickly deteriorated as shown by a large increase in membrane resistance. The AZO/TiO_2 membranes had enhanced resistance to biofouling, with a 72% reduction in bacterial counts in the absence of an applied current due to its higher hydrophilicity than the bare polymeric membrane, and it achieved an additional 50% reduction in bacterial colonization with an applied voltage. The use of TiO_2-capped AZO layers provides a new approach for producing conductive membranes using abundant materials, and it avoids the risk of releasing nanoparticles into the environment.

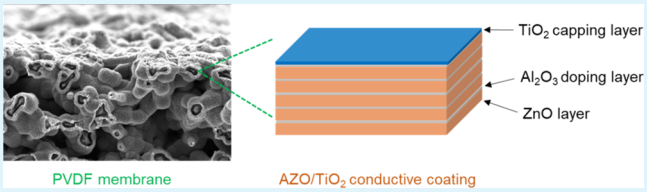

KEYWORDS: *water treatment, conductive membrane, anti-biofouling, aluminum-doped zinc oxide conductive coating, atomic layer deposition*

1. INTRODUCTION

Polymeric membranes have been widely used in water treatment processes for filtration, separation, and desalination.[1,2] Membranes can be made with different pore sizes to efficiently separate large bacteria or small ions from water and provide stable effluent quality.[2] Despite wide applications of membranes in many processes, membrane fouling is inevitable over time which eventually increases operational costs.[3,4] Biofouling is ubiquitous in membrane-based applications ranging from microfiltration to reverse osmosis.[5,6] The growth of biofilms can block membrane pores, which results in a reduced water flux and higher backpressures that increase energy consumption.[7,8]

The development of electrically conductive membranes over the past few years is a new and promising strategy for reducing membrane fouling.[9,10] Applying a low voltage to a conductive membrane (less than 2 V) can reduce bacterial attachment, leading to better control on adhesion of bacteria and growth of biofilms.[11,12] The mechanism behind reduced biofouling is charge repulsion through creating a negatively charged surface, as the outer membrane of most bacteria is also negatively charged, and thus application of a low voltage is sufficient to reduce initial bacterial attachment.[13] Current generation can also drive other reactions, such as hydrogen evolution or oxygen reduction, that can reduce inorganic and organic fouling.[11] Nanomaterials such as carbon nanotubes (CNTs) or graphene particles are usually used to produce an electrically conductive coating on the membrane by pressure filtration or spraying.[14−16] However, the use of CNTs or graphene nanomaterials requires the use of binders to form the conductive layer, and thus poor binding of the particles risks possible leaching of the nanoparticles into the environment.[17] Although cross-linking of the CNT or graphene layers using binders stabilizes the particles in these conductive layers, the use of these binders adds additional chemical costs and it can require complicated and expensive fabrication procedures. Conductive membranes therefore demonstrate great potential for addressing the challenge of membrane fouling, but alternative procedures with less chemical usage and stable coatings are needed to advance this approach into more practical applications.

Atomic layer deposition (ALD) is a useful technique for producing highly uniform and thin coatings of various metals on many different substrates at the atomic scale.[18,19] ALD is

Received: November 9, 2019
Accepted: December 13, 2019
Published: December 13, 2019

DOI: 10.1021/acsami.9b20385
ACS Appl. Mater. Interfaces 2020, 12, 963−969

usually performed with multiple layers to produce coatings with different thicknesses. During the first ALD cycle, a precursor is initially chemisorbed onto the substrate surface to form one monolayer, followed by a second precursor that is chemisorbed and reacted with the first precursor to accomplish one atomic layer of deposition.[20] The cycles are then repeated to reach a desired thickness, and the subsequently deposited materials are continuously bonded to the previous layer without an additional cross-linking process or chemical consumption, producing functional membranes with highly controlled characteristics.[20] Aluminum-doped zinc oxide (AZO) is a highly conductive metal oxide composite consisting of inexpensive and abundant aluminum oxide and zinc oxide materials, which have been used as the electron transport layer in many applications, such as solar cells and organic light-emitting devices.[21] An aluminum doping of 1−10% (wt) into zinc oxide can effectively boost electron transport efficiency and lead to a low resistance of an AZO layer.[22] A low sheet resistance can easily be obtained using multiple AZO layers, for example, 24 Ω/sq (ohm/square) for a 250 nm-thick film of AZO on a nonconductive glass substrate.[23] The resistance is comparable to or lower than that of CNTs or graphene coatings on membranes, which range from 59 to 778 Ω/sq.[12,24,25] Although AZO films can have very low surface resistances, they all suffer from OH^--induced corrosion[26] and therefore are a lack of sufficient stability for water-based applications without other modifications.

In this work, TiO_2-capped AZO was explored as a material to produce an electrically conductive layer on the polyvinylidene fluoride (PVDF) microfiltration membrane. Multiple AZO layers with different thicknesses were deposited on PVDF membranes to investigate the impact of the layer thickness on membrane resistance and electrochemical properties. An ultrathin titanium oxide (TiO_2) capping layer was added on top of the final AZO layer to prevent the decomposition of the AZO layer over time. Water permeability and antibiofouling performance of the AZO/TiO_2 membranes were further evaluated in customized membrane cells and compared to the performance of the bare membranes and AZO-only coated membranes (no TiO_2 capping layer).

2. EXPERIMENTAL SECTION

2.1. AZO/TiO_2 Membrane Fabrication. Commercial PVDF microfiltration membranes (0.22 μm, hydrophilic, Millipore, USA) used as the base membranes were rinsed with deionized (DI) water and vacuum-dried for 8 h at 60 °C to remove residual water. No change in the pore structure of the PVDF membranes after drying was observed possibly because of the rigid nature of the PVDF polymer and the relatively large membrane pore size. The membranes were placed into an ALD chamber (Savannah 200, Veeco-CNT, USA), preheated under vacuum (~0.2 Torr) at 120 °C for 30 min, and then maintained at 120 °C during the ALD process. The temperature of 120 °C was selected to both ensure high deposition quality and prevent deformation of the PVDF membrane. One complete layer of AZO consisted of depositing twenty cycles of zinc oxide (ZnO) followed by one cycle of aluminum oxide (Al_2O_3), achieving a ratio of ZnO/Al_2O_3 of 20:1. Different thicknesses of AZO were obtained by repeating 25 (AZO25), 37 (AZO37), or 50 (AZO50) layers.

Each ZnO deposition cycle consisted of: (1) pulsing diethyl zinc ($Zn(C_2H_5)_2$, Sigma-Aldrich, USA) vapor into the chamber for 0.02 s, (2) purging for 30 s with Ar gas (99.999997%) to remove excess precursor, (3) pulsing water (H_2O) vapor into the chamber for 0.02 s to react with the chemisorbed diethyl zinc, and (4) purging Ar gas for 30 s to remove excess H_2O. The Al_2O_3 deposition cycle was similarly conducted by replacing the diethyl zinc with trimethyl aluminum ($Al(CH_3)_3$, Sigma-Aldrich, USA) in the previous steps. The chemical reactions of $Zn(C_2H_5)_2$ and $Al(CH_3)_3$ with H_2O are[27,28]

$$ZnOH^* + Zn(CH_2CH_3)_2 \rightarrow ZnOZn(CH_2CH_3)^* + CH_3CH_3 \quad (1)$$

$$Zn(CH_2CH_3)^* + H_2O \rightarrow ZnOH^* + CH_3CH_3 \quad (2)$$

$$AlOH^* + Al(CH_3)_3 \rightarrow AlOAl(CH_3)_2^* + CH_4 \quad (3)$$

$$AlCH_3^* + H_2O \rightarrow AlOH^* + CH_4 \quad (4)$$

where the asterisk denotes the surface species.

A capping layer of TiO_2 was deposited on the final AZO layer in the ALD chamber by applying 100 cycles of TiO_2. The deposition of TiO_2 was similar to that of ZnO, except that the purging time of the tetrakis(dimethylamido)titanium(IV) (TDMAT) precursor was 0.3 s, and H_2O vapor exposure was adjusted to 0.02 s because of the low vapor pressure of TDMAT. The TiO_2 reactions were[29]

$$Ti(N(CH_3)_2)_4 + TiO_2OH^* \rightarrow TiO_2OTi(N(CH_3)_2)_3^* + NH(CH_3)_2 \quad (5)$$

$$TiO_2OTi(N(CH_3)_2)_3^* + 2H_2O \rightarrow TiO_2TiO_2OH^* + 3NH(CH_3)_2 \quad (6)$$

where the asterisk denotes the surface species. The TiO_2 capping layer (~11 nm) was added on all AZO final layers except otherwise noted. The fabricated membranes were stored at 4 °C prior to use. Silicon wafers (001) were used as the reference substrate, and the coating thickness on the wafer was determined by using a Woollam M-2000F Focused Beam Spectroscopic Ellipsometer (J.A. Woollam Co. USA).

2.2. Surface Characterization. X-ray photoelectron spectroscopy (XPS) (Axis Ultra XPS, Kratos Analytical, UK, monochrome Al Kα source, 1486 eV) was performed on plain PVDF and TiO_2-capped AZO50 membranes at a sampling depth of 3−6 nm. CASA XPS software was used for the elemental and peak-fitting analysis.

Scanning electron microscopy (SEM; Nova NanoSEM 630, FEI Company, USA) was conducted to examine the surface and cross-section morphology of the plain and AZO membranes. Samples for cross-section SEM analyses were prepared by immersing membranes into liquid nitrogen for 15 s and then breaking the membrane in liquid nitrogen using tweezers to prevent mechanical deformation of the samples. To avoid charging effects on the nonconductive plain PVDF membrane, the plain membrane samples were sputter-coated with 10 nm of iridium prior to SEM analysis. AZO membranes were directly imaged without additional iridium coating.

The surface topology of the prepared membranes was characterized with an optical profilometry technique using a 3D optical surface profiler (Nexview NX2, Zygo Corporation, USA). The surface data were collected using a 50× objective with a 2× internal magnification. The sampling area was 88 × 88 μm^2, and at least two sites were sampled to ensure accuracy. The data were then collected and analyzed by Mx Software.

Contact angle measurements (duplicate) were conducted using an automated goniometer/tensiometer (model 260, Ramé-hart Instrument Co. USA). A membrane specimen was placed on a sample stage, and a 5 μL droplet of DI water was dropped on the membrane by using a syringe equipped with a 100 μL pipette tip. The images were captured and analyzed (DROPimage Advanced software) to obtain the contact angle by a geometrical method (sessile drop).

2.3. Electrochemical Characterization. The sheet resistances of the AZO membranes were determined using a four-point probe station (Summit 12861, Cascade Microtech, USA). An average sheet resistance was obtained from at least four measurements on each sample. For the aqueous stability test, AZO50 membranes with and without the TiO_2 capping layer were immersed into DI water at room temperature for 7 days, and the sheet resistances for both membranes were measured daily. The AZO50 membranes with the TiO_2 capping layer were also put in an ultrasonication bath (Branson 2510, USA)

DOI: 10.1021/acsami.9b20385
ACS Appl. Mater. Interfaces 2020, 12, 963−969

for 0.5 h to test their physical stability. The sheet resistance of the AZO50 membranes was checked both before and after sonication.

The electrochemical performance of AZO membranes was evaluated using cyclic voltammetry (CV) in an electrochemical cell (4 cm length, 3 cm diameter).[30] The electrolyte was 50 mM sodium chloride (NaCl), and the counter electrode was a 7 cm^2 round platinum plate. An Ag/AgCl reference electrode (RE-5B, BASi, West Lafayette, IN; +0.209 V vs a standard hydrogen electrode, SHE) was placed close to the membranes and kept in the same position for all tests. All potentials were reported versus SHE. A potentiostat (VMP3 Multichannel Workstation, Biologic Science Instruments, USA) was used for all measurements, and all tests were conducted in a constant temperature room (30 °C). The potentials on the membranes were scanned from +1 to −1 V versus SHE for five times to reach steady conditions.

2.4. Membrane Performance Characterization. Water flux (LMH, L m^{-2} h^{-1}) through the membranes was obtained using a stirred cell (model 8010, Millipore, USA) with an effective membrane area of 4.1 cm^2. DI water was used as the feed solution, and the cell was pressurized at 2 psi using nitrogen gas. The membranes were prewashed with 90% isopropanol and 10% DI water prior to tests to remove any chemical residues from membrane fabrication. Water flux was also measured with a 0.1 μm pore-diameter PVDF membrane (Millipore, USA) as an additional reference. Duplicate tests were conducted for all membranes. The membrane porosity was measured using a typical wet-dry method as previously described.[31] The membranes were first immersed in DI water overnight and weighed after removing excessive water with filter papers. The membranes were then dried in a vacuum oven for 24 h at 80 °C and weighed again. The porosity P was calculated as follows

$$P\ (\%) = \frac{W_w - W_d}{Ah} \times 1000$$

where W_w and W_d are the weights of the wet and dry membranes (g), A is the membrane surface area (cm^2), and h is the membrane thickness (mm). The membrane porosity was measured two times and average values were reported.

Bacterial attachment tests were performed in a customized flow cell (Figure S1). This cell consisted of a single channel 1 mm in height and an effective membrane area of 7 cm^2 (membrane diameter of 3 cm), with a titanium foil counter electrode at the upper channel wall. *Pseudomonas aeruginosa*, used as the model microorganism, was cultured in Luria Bertani broth, as previously described.[32] The feed solution contained 10^8 CFU/mL and 50 mM NaCl. Experiments were performed under crossflow conditions (no permeation) at a feed solution rate of 2 mL/min using a peristaltic pump at 30 °C.[11] The flow cell was operated for 3 h in the continuous mode with recirculation. A potentiostat (VMP3 Multichannel Workstation, Bio-Logic Science Instruments, USA) was used to apply −1 V whole cell voltage with the membrane as the working electrode. After the experiment, the membranes were taken out and sonicated in 10 mL of 0.9% (wt) NaCl solution for 10 min to detach bacterial cells. Cells were then stained with 5.01 μM SYTO 9 and 30 μM propidium iodide (Live/Dead Baclight Bacterial Viability Kit, Thermo Fisher, USA) and counted on black filters using a fluorescence microscope (BX61, Olympus).[33] The total bacterial counts were then averaged based on at least 10 sampling fields.

3. RESULTS AND DISCUSSION

3.1. Aqueous Stability of AZO Membranes. With a thin capping layer of TiO_2, the AZO50 membrane showed almost no change in sheet resistance in DI water over time. The sheet resistance of the AZO50 membrane with the TiO_2 capping layer was 72 ± 4 Ω/sq on day 1 and did not appreciably change after 7 days (75 ± 3 Ω/sq), demonstrating its high stability in aqueous solutions (Figure 1A). In contrast, the PVDF membrane coated with 50 cycles of AZO and no TiO_2 capping layer showed a rapid increase in sheet resistance when

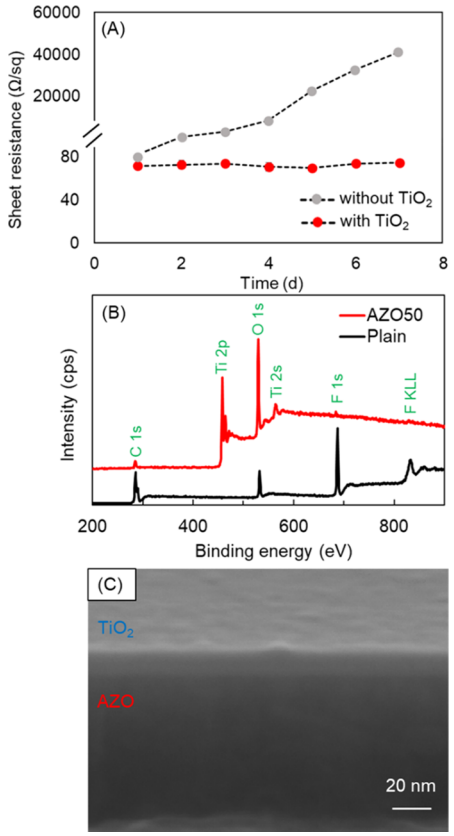

Figure 1. (A) Sheet resistance change in water over 7 days for AZO50 membranes with and without the TiO_2 capping layer; (B) XPS spectra for plain (0.22 μm) and AZO50 membranes capped with TiO_2; and (C) SEM image of TiO_2 and AZO layers on the silicon wafer.

immersed in DI water. The initial sheet resistance of the AZO50 membrane without TiO_2 was 80 ± 3 Ω/sq, and it quickly increased to 8600 ± 10 Ω/sq four days after immersion in DI water (Figure 1A). The sheet resistance further increased to 41 000 ± 10 Ω/sq at day 7, which was more than 500 times compared to the initial resistance, suggesting the extreme instability of AZO in aqueous solution. This result showing large increases in resistance for AZO exposed to DI water was consistent with previous studies where AZO coatings had increased resistance with only exposure to humidified air, which mainly resulted from formation of hydroxides.[26,34] The TiO_2 capping layer could effectively prevent exposure of water molecules to the AZO layer,[35] therefore greatly enhancing the aqueous stability of AZO. In addition, the AZO50 membranes also exhibited excellent physical stability with no change in the sheet resistance after sonication (Figure S2).

The complete shielding of the AZO surface by TiO_2 was further confirmed based on surface elemental analysis using XPS. For the AZO50 membrane capped with TiO_2, Ti 2p (458.55 eV) was detected and the O 1s (530.07 eV) signal was further boosted, demonstrating the successful deposition of TiO_2 (Figure 1B). No zinc or aluminum peaks were detected because of the complete coverage of the AZO by TiO_2. The C 1s and F 1s peaks were also significantly suppressed, suggesting the shielding effect from TiO_2 capping. The plain PVDF membrane showed signature peaks at C 1s (284.8 eV) and F 1s (684.07 eV) (Figure 1B), which corresponded well with the chemical structure of PVDF containing C−C and C−F bonds. The detection of PVDF for the AZO50 membrane capped

DOI: 10.1021/acsami.9b20385
ACS Appl. Mater. Interfaces 2020, 12, 963−969

with TiO_2 indicated the existence of some uncovered membrane locations, which might result from diffusion hindrance or partially low surface affinity of the precursor vapors. Oxygen was detected possibly because of some hydrophilic additives used during commercial membrane fabrication. SEM also identified a uniform capping layer of TiO_2 on top of AZO (Figure 1C). Therefore, capping AZO with TiO_2 demonstrated an effective strategy in stabilizing AZO for aqueous applications.

3.2. Electrochemical Properties of AZO Membranes. The sheet resistances of the AZO membranes significantly decreased in proportion to deposition thickness of the AZO layers. With 25 layers, the TiO_2-capped AZO25 had a final coating thickness of 61 ± 4 nm and a sheet resistance of 480 ± 30 Ω/sq (Figure 2A). Increasing the AZO layers decreased the resistance to 130 ± 10 Ω/sq (79 ± 1 nm thick) for 37 layers and to 67 ± 10 Ω/sq (116 ± 10 nm thick) for 50 layers. Thus, increasing the thickness of the coating 1.9 times decreased the resistance by 7 times (Figure 2A). This lowered sheet resistance corresponded well with general findings that increasing the AZO thickness could provide a greater number of charge carriers resulting in reduced resistance.[36] The resistance range obtained here was comparable to typical CNTs or graphene membranes (59 to 778 Ω/sq),[24,25] demonstrating a similar effectiveness of the AZO for fabricating conductive membranes as those using these other materials.

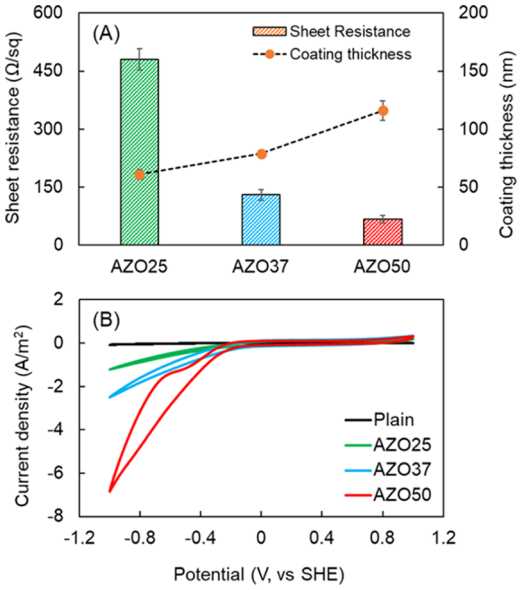

Figure 2. (A) Sheet resistances and coating thickness for PVDF membranes coated with AZO/TiO_2 at 25, 37, and 50 cycles and (B) CV curves for plain (0.22 μm), AZO25, AZO37, and AZO50 membranes with TiO_2 capping scanning at 1 mV/s from 1 to −1 V (vs SHE).

Analysis of the AZO membranes using CV showed higher current densities with increasing AZO deposition thickness. The AZO50 membrane showed the highest current density of 6.6 A/m^2 at −1 V (vs SHE), which was 4.5 times higher than 1.2 A/m^2 obtained for AZO25 (Figure 2B). No current was measured for the plain PVDF membrane, consistent with its nonconductive nature. The reduction peaks observed with the AZO coating were attributed to the oxygen reduction reaction catalyzed by TiO_2 at the capping layer, as this metal oxide has previously been studied as an oxygen reduction catalyst.[37]

3.3. Surface Morphology. The AZO membranes had a uniform AZO coating along the PVDF fibrous structure. With a thicker AZO coating, the surface pores of the AZO membrane became smaller compared to the plain PVDF membrane, in the order of the applied layers (25, 37, and 50) (Figure 3A–D), which would adversely impact water flux at a fixed applied pressure. A unique shell structure was observed in the cross-section SEM, where the AZO coating was deposited along the PVDF fibers without blocking the pores (Figure 3E–H). This is different from the situation using nanotubes or graphene coatings. Typical CNT-coated conductive membranes usually fully retain a porous layer of CNTs on the top surface of membranes that could potentially trap foulants in water, which might alter the filtration properties of the conductive membrane compared to the original membrane.[24] Because the AZO coating was deposited as atomic monolayers, it was deposited on the surface of pore walls, utilizing the intrinsic topography of membranes as a template, rather than covering the pores. Thus, this vapor deposition approach provided a much different type of membrane as it impacted the

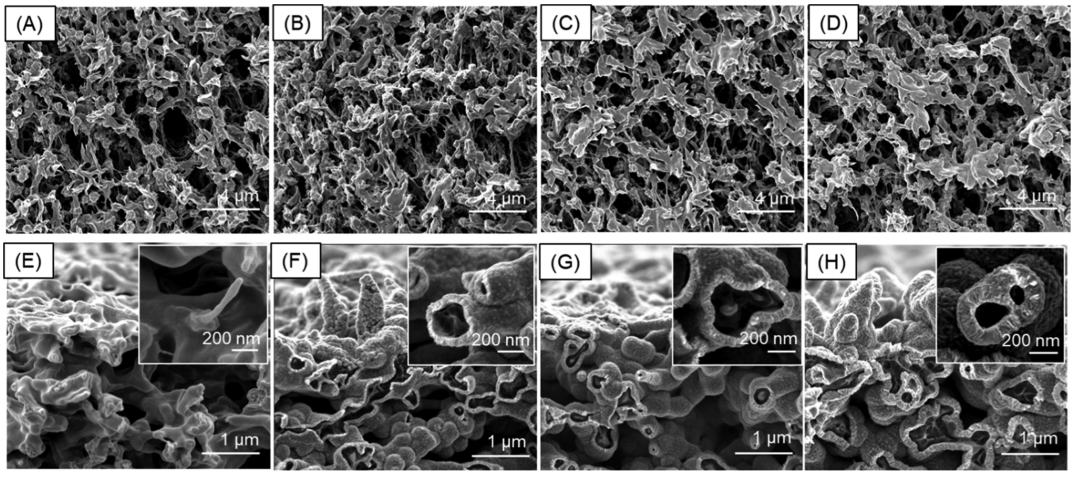

Figure 3. (A–D) Surface morphology and (E–H) cross-section morphology for (A,E) plain (0.22 μm), (B,F) AZO25, (C,G) AZO37, and (D,H) AZO50 membranes.

DOI: 10.1021/acsami.9b20385
ACS Appl. Mater. Interfaces 2020, 12, 963–969

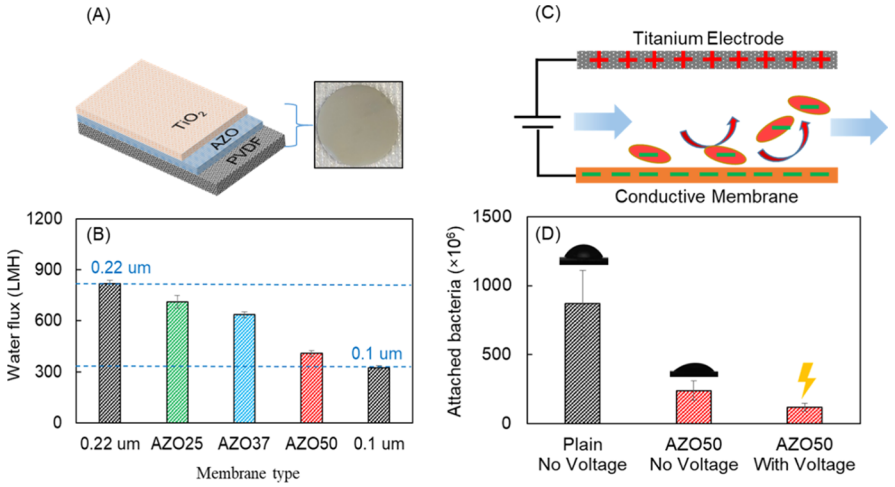

Figure 4. (A) Structure scheme of the TiO_2-capped conductive AZO-PVDF membrane; (B) water fluxes for 0.22 μm plain, AZO25, AZO37, AZO50, and 0.1 μm plain membranes at an applied pressure of 2 psi; (C) scheme illustration of antibacterial attachment with AZO conductive membrane under externally applied voltage; and (D) attached bacterial number on plain (0.22 μm) and AZO50 membranes with or without an applied voltage of −1 V.

pore sizes to a much lesser extent than CNT membranes. The membrane surface topology was not significantly affected by the AZO coatings possibly because of the inherent rough topology of the microporous PVDF membranes (Figure S4).

3.4. Membrane Performance. The deposited AZO coating along the PVDF fibrous structure increased the pore wall thickness, narrowing the membrane channels but not completely covering them, so that the water flux decreased with the number of AZO layers (Figure 4A). The AZO25 membrane with a 61 nm coating thickness showed a pure water flux of 710 ± 40 LMH, which was only 13% lower than 820 ± 20 LMH obtained for a plain 0.22 μm PVDF membrane (Figure 4B). Further increases in the coating thickness to 79 nm for the AZO37 membrane decreased the water flux to 640 ± 20 LMH, and a membrane thickness of 116 nm for the AZO50 membrane had a water flux of 410 ± 20 LMH or about half of that for the plain 0.22 μm PVDF membrane. This reduced flux was consistent with the decreased porosity for AZO membranes (61 ± 2% for AZO25, 57 ± 3% for AZO37, and 43 ± 3% for AZO25) compared to the plain 0.22 μm PVDF membrane (75 ± 4%) (Figure S3). The fluxes of AZO membranes were still above the recommended filtration flux of 50−100 LMH for typical microfiltration conditions so that the membranes were not operated at the maximum flux to avoid severe fouling and more frequent cleaning.[38]

In spite of flux decrease relative to the 0.22 μm PVDF membrane, the AZO membranes still had a higher water flux than a PVDF membrane with a nominal pore diameter of 0.1 μm (Figure 4B). Conventional CNT membranes usually have CNT coatings of one to several microns to achieve a desired conductivity because of contact resistance between CNTs,[24,25] but the AZO membranes required only tens of nanometers owing to the conformal coating from the ALD technique.

3.5. Antifouling Properties. The AZO50 membrane with the TiO_2 capping layer showed the least fouling when a low voltage was applied to the membrane. After flowing by 10^8 CFU/mL *P. aeruginosa* in a customized membrane cell (Figures 4C and S1) for 3 h, the AZO50 membrane surface had 1.2 ± 0.3 × 10^8 cell counts with applied −1 V of the whole cell voltage, which was 50% lower than 2.4 ± 0.5 × 10^8 on the AZO50 membrane surface without applying any voltage (Figure 4D). This additional reduction in surface bacterial counts with an applied current was due to the electric repulsion that reduced bacterial attachment, which was similarly demonstrated using CNT membranes where over 90% reduction in bacteria on the membrane surface was reported when applying a voltage of 1.5 V.[11] Even without applying any voltage, the AZO50 membrane still had 72% reduction in bacterial attachment compared to the plain PVDF membrane with 8.7 ± 2 × 10^8 cell counts (Figure 4D), mainly resulting from the TiO_2 capping layer altering the surface hydrophilicity to lower bacterial attachment. The plain PVDF membrane had a contact angle of 56°, which was larger than 35° for the AZO50 membrane (Figure 4D), suggesting the increased surface hydrophilicity for the AZO membrane. Increasing the membrane hydrophilicity by blending in TiO_2 particles had been previously studied to improve membrane fouling resistance,[39] consistent with our findings. The AZO50 membrane showed good antibiofouling properties with combined advantages of enhanced hydrophilicity and electrical repulsion of negatively charged bacteria, with a total 86% reduction in bacterial cell attachment on the membrane surface compared to the unmodified plain PVDF membrane (Figure 4D). The AZO50 membrane showed a relatively decreased flux, but it still was operating above a typical operation flux used for microfiltration.[38] Thus, this more conductive AZO50 membrane is most promising to hinder antibiofouling because of the stronger electric field to repel bacteria. The electrically polarized membranes can reduce the amount and frequency of additional chemical dosing of sodium hydroxide or sodium dodecyl sulfate in conventional biofouling control,[40] providing a viable antibiofouling strategy to hinder biofouling and simplifying the membrane care procedure.

4. CONCLUSIONS

The addition of a TiO_2 capping layer on AZO was originally conducted to enhance the aqueous stability of AZO and maintain well the electron transport properties. The TiO_2-capped AZO membrane demonstrated a stable constant sheet resistance (~75 Ω/sq) over 7 days, while the non-capped AZO membrane quickly became unstable as shown by the sheet resistance increasing from 80 ± 3 to 41 200 ± 10 Ω/sq after 7

DOI: 10.1021/acsami.9b20385
ACS Appl. Mater. Interfaces 2020, 12, 963−969

days immersion in DI water. Increasing the thickness of AZO/TiO_2 composite coating from 61 to 116 nm lowered the sheet resistance from 480 ± 30 to 67 ± 10 Ω/sq. The water flux for AZO membranes decreased inversely with the increasing thickness of AZO coating because of narrowed pore channels. The AZO membranes also showed good antibiofouling properties with an 86% reduction in total bacterial cell attachment on the membrane surface compared to an unmodified plain PVDF membrane, possibly because of both surface hydrophilicity enhancement and charge repulsion with an applied current. Taken together, these results show that the atomic layer-deposited TiO_2-capped AZO conductive layer is a simple method to fabricate conductive membranes that maintain a pore structure, with the pore size decreasing in proportion to the thickness of the applied coating. The atomic scale tuning of membrane pores by ALD also offered an engineering pathway to tailor membrane pore sizes for targeted applications. Further examination of this conductive membrane in practical water treatment is still needed to evaluate the separation performance and operation principles.

■ ASSOCIATED CONTENT

Supporting Information

The Supporting Information is available free of charge at https://pubs.acs.org/doi/10.1021/acsami.9b20385.

Customized membrane flow cell; sheet resistances of AZO50 membranes; porosity of 0.22 μm plain, AZO25, AZO37, and AZO50 membranes; membrane thicknesses; optical profilometry surface images; and XPS spectra (PDF)

■ AUTHOR INFORMATION

Corresponding Author

*E-mail: blogan@psu.edu. Phone: +1 814 863 7908. Fax: +1 814 863 7304.

ORCID

Moon Son: 0000-0002-3770-148X

Bruce E. Logan: 0000-0001-7478-8070

Notes

The authors declare no competing financial interest.

■ ACKNOWLEDGMENTS

The authors thank Dr. Manish Kumar's lab at The Pennsylvania State University for providing the dead-end filtration test device. This research was supported by the King Abdullah University of Science and Technology (KAUST) (OSR-2017-CPF-2907-02) and Penn State University.

■ REFERENCES

(1) Pendergast, M. M.; Hoek, E. M. V. A Review of Water Treatment Membrane Nanotechnologies. *Energy Environ. Sci.* **2011**, *4*, 1946−1971.

(2) Van der Bruggen, B.; Vandecasteele, C.; Van Gestel, T.; Doyen, W.; Leysen, R. A Review of Pressure-Driven Membrane Processes in Wastewater Treatment and Drinking Water Production. *Environ. Prog.* **2003**, *22*, 46−56.

(3) Guo, W.; Ngo, H.-H.; Li, J. A Mini-Review on Membrane Fouling. *Bioresour. Technol.* **2012**, *122*, 27−34.

(4) Vrouwenvelder, J. S.; Van Loosdrecht, M. C. M.; Kruithof, J. C. Early Warning of Biofouling in Spiral Wound Nanofiltration and Reverse Osmosis Membranes. *Desalination* **2011**, *265*, 206−212.

(5) Vrouwenvelder, J. S.; Manolarakis, S. A.; Van der Hoek, J. P.; Van Paassen, J. A. M.; van der Meer, W. G. J.; Van Agtmaal, J. M. C.; Prummel, H. D. M.; Kruithof, J. C.; Van Loosdrecht, M. C. M. Quantitative Biofouling Diagnosis in Full Scale Nanofiltration and Reverse Osmosis Installations. *Water Res.* **2008**, *42*, 4856−4868.

(6) Kang, S.; Subramani, A.; Hoek, E.; Deshusses, M.; Matsumoto, M. Direct Observation of Biofouling in Cross-flow Microfiltration: Mechanisms of Deposition and Release. *J. Membr. Sci.* **2004**, *244*, 151−165.

(7) Abdul Azis, P. K.; Al-Tisan, I.; Sasikumar, N. Biofouling Potential and Environmental Factors of Seawater at A Desalination Plant Intake. *Desalination* **2001**, *135*, 69−82.

(8) Bucs, S. S.; Farhat, N.; Kruithof, J. C.; Picioreanu, C.; van Loosdrecht, M. C. M.; Vrouwenvelder, J. S. Review on Strategies for Biofouling Mitigation in Spiral Wound Membrane Systems. *Desalination* **2018**, *434*, 189−197.

(9) de Lannoy, C. F.; Jassby, D.; Davis, D. D.; Wiesner, M. R. A Highly Electrically Conductive Polymer−Multiwalled Carbon Nanotube Nanocomposite Membrane. *J. Membr. Sci.* **2012**, *415*−*416*, 718−724.

(10) Ahmed, F.; Lalia, B. S.; Kochkodan, V.; Hilal, N.; Hashaikeh, R. Electrically Conductive Polymeric Membranes for Fouling Prevention and Detection: A Review. *Desalination* **2016**, *391*, 1−15.

(11) Thamaraiselvan, C.; Ronen, A.; Lerman, S.; Balaish, M.; Ein-Eli, Y.; Dosoretz, C. G. Low Voltage Electric Potential as A Driving Force to Hinder Biofouling in Self-Supporting Carbon Nanotube Membranes. *Water Res.* **2018**, *129*, 143−153.

(12) Ronen, A.; Duan, W.; Wheeldon, I.; Walker, S.; Jassby, D. Microbial Attachment Inhibition Through Low-Voltage Electrochemical Reactions on Electrically Conducting Membranes. *Environ. Sci. Technol.* **2015**, *49*, 12741−12750.

(13) de Lannoy, C.-F.; Jassby, D.; Gloe, K.; Gordon, A. D.; Wiesner, M. R. Aquatic Biofouling Prevention by Electrically Charged Nanocomposite Polymer Thin Film Membranes. *Environ. Sci. Technol.* **2013**, *47*, 2760−2768.

(14) Gao, G.; Zhang, Q.; Hao, Z.; Vecitis, C. D. Carbon Nanotube Membrane Stack for Flow-Through Sequential Regenerative Electro-Fenton. *Environ. Sci. Technol.* **2015**, *49*, 2375−2383.

(15) Dudchenko, A. V.; Chen, C.; Cardenas, A.; Rolf, J.; Jassby, D. Frequency-Dependent Stability of CNT Joule Heaters in Ionizable Media and Desalination Processes. *Nat. Nanotechnol.* **2017**, *12*, 557.

(16) Hu, C.; Liu, Z.; Lu, X.; Sun, J.; Liu, H.; Qu, J. Enhancement of The Donnan Effect Through Capacitive Ion Increase Using an Electroconductive rGO-CNT Nanofiltration Membrane. *J. Mater. Chem. A* **2018**, *6*, 4737−4745.

(17) Liu, Q.; Qiu, G.; Zhou, Z.; Li, J.; Amy, G. L.; Xie, J.; Lee, J. Y. An Effective Design of Electrically Conducting Thin-Film Composite (TFC) Membranes for Bio And Organic Fouling Control in Forward Osmosis (FO). *Environ. Sci. Technol.* **2016**, *50*, 10596−10605.

(18) George, S. M. Atomic Layer Deposition: An Overview. *Chem. Rev.* **2010**, *110*, 111−131.

(19) Leskelä, M.; Ritala, M. Atomic Layer Deposition Chemistry: Recent Developments and Future Challenges. *Angew. Chem., Int. Ed.* **2003**, *42*, 5548−5554.

(20) Zhou, X.; Zhao, Y.-Y.; Kim, S.-R.; Elimelech, M.; Hu, S.; Kim, J.-H. Controlled TiO2 Growth on Reverse Osmosis and Nanofiltration Membranes by Atomic Layer Deposition: Mechanisms and Potential Applications. *Environ. Sci. Technol.* **2018**, *52*, 14311−14320.

(21) Zhao, X.; Shen, H.; Zhang, Y.; Li, X.; Zhao, X.; Tai, M.; Li, J.; Li, J.; Li, X.; Lin, H. Aluminum-Doped Zinc Oxide as Highly Stable Electron Collection Layer for Perovskite Solar Cells. *ACS Appl. Mater. Interfaces* **2016**, *8*, 7826−7833.

(22) Banerjee, P.; Lee, W.-J.; Bae, K.-R.; Lee, S. B.; Rubloff, G. W. Structural, Electrical, and Optical Properties of Atomic Layer Deposition Al-Doped ZnO Films. *J. Appl. Phys.* **2010**, *108*, 043504.

(23) Chen, T. L.; Ghosh, D. S.; Krautz, D.; Cheylan, S.; Pruneri, V. Highly Stable Al-Doped ZnO Transparent Conductors Using an Oxidized Ultrathin Metal Capping Layer at Its Percolation Thickness. *Appl. Phys. Lett.* **2011**, *99*, 093302.

(24) Zhang, Q.; Arribas, P.; Remillard, E. M.; García-Payo, M. C.; Khayet, M.; Vecitis, C. D. Interlaced CNT Electrodes for Bacterial

DOI: 10.1021/acsami.9b20385
ACS Appl. Mater. Interfaces 2020, 12, 963−969

Fouling Reduction of Microfiltration Membranes. *Environ. Sci. Technol.* **2017**, *51*, 9176−9183.
(25) Tang, L.; Iddya, A.; Zhu, X.; Dudchenko, A. V.; Duan, W.; Turchi, C.; Vanneste, J.; Cath, T. Y.; Jassby, D. Enhanced Flux and Electrochemical Cleaning of Silicate Scaling on Carbon Nanotube-Coated Membrane Distillation Membranes Treating Geothermal Brines. *ACS Appl. Mater. Interfaces* **2017**, *9*, 38594−38605.
(26) Litzov, I.; Azimi, H.; Matt, G.; Kubis, P.; Stubhan, T.; Popov, G.; Brabec, C. J. Accelerated Degradation of Al3+ Doped ZnO Thin Films Using Damp Heat Test. *Org. Electron.* **2014**, *15*, 569−576.
(27) Widjaja, Y.; Musgrave, C. B. Quantum Chemical Study of the Mechanism of Aluminum Oxide Atomic Layer Deposition. *Appl. Phys. Lett.* **2002**, *80*, 3304−3306.
(28) Elam, J. W.; George, S. M. Growth of ZnO/Al2O3 Alloy Films Using Atomic Layer Deposition Techniques. *Chem. Mater.* **2003**, *15*, 1020−1028.
(29) Xie, Q.; Jiang, Y.-L.; Detavernier, C.; Deduytsche, D.; Van Meirhaeghe, R. L.; Ru, G.-P.; Li, B.-Z.; Qu, X.-P. Atomic Layer Deposition of Ti O 2 from Tetrakis-Dimethyl-Amido Titanium or Ti Isopropoxide Precursors and H 2 O. *J. Appl. Phys.* **2007**, *102*, 083521.
(30) Hou, J.; Liu, Z.; Yang, S.; Zhou, Y. Three-Dimensional Macroporous Anodes Based on Stainless Steel Fiber Felt for High-Performance Microbial Fuel Cells. *J. Power Sources* **2014**, *258*, 204−209.
(31) Celik, E.; Liu, L.; Choi, H. Protein Fouling Behavior of Carbon Nanotube/Polyethersulfone Composite Membranes During Water Filtration. *Water Res.* **2011**, *45*, 5287−5294.
(32) Singh, S. P.; Li, Y.; Be'er, A.; Oren, Y.; Tour, J. M.; Arnusch, C. J. Laser-Induced Graphene Layers and Electrodes Prevents Microbial Fouling and Exerts Antimicrobial Action. *ACS Appl. Mater. Interfaces* **2017**, *9*, 18238−18247.
(33) Perreault, F.; De Faria, A. F.; Nejati, S.; Elimelech, M. Antimicrobial Properties of Graphene Oxide Nanosheets: Why Size Matters. *ACS Nano* **2015**, *9*, 7226−7236.
(34) Tohsophon, T.; Hüpkes, J.; Calnan, S.; Reetz, W.; Rech, B.; Beyer, W.; Sirikulrat, N. Damp Heat Stability and Annealing Behavior of Aluminum Doped Zinc Oxide Films Prepared by Magnetron Sputtering. *Thin Solid Films* **2006**, *511*−*512*, 673−677.
(35) Shan, C. X.; Hou, X.; Choy, K.-L. Corrosion Resistance of TiO2 Films Grown on Stainless Steel by Atomic Layer Deposition. *Surf. Coat. Technol.* **2008**, *202*, 2399−2402.
(36) Silva, É. P. d.; Chaves, M.; Durrant, S. F.; Lisboa-Filho, P. N.; Bortoleto, J. R. R. Morphological and Electrical Evolution of ZnO: Al Thin Filmsdeposited by RF Magnetron Sputtering onto Glass Substrates. *Mater. Rep.* **2014**, *17*, 1384−1390.
(37) Baez, V. B.; Graves, J. E.; Pletcher, D. The Reduction of Oxygen on Titanium Oxide Electrodes. *J. Electroanal. Chem.* **1992**, *340*, 273−286.
(38) Olabarrieta, J.; Monzón, O.; Belaustegui, Y.; Alvarez, J.-I.; Zorita, S. Removal of TiO2 Nanoparticles From Water by Low Pressure Pilot Plant Filtration. *Sci. Total Environ.* **2018**, *618*, 551−560.
(39) Oh, S. J.; Kim, N.; Lee, Y. T. Preparation and Characterization of PVDF/TiO2 Organic−Inorganic Composite Membranes for Fouling Resistance Improvement. *J. Membr. Sci.* **2009**, *345*, 13−20.
(40) Creber, S. A.; Vrouwenvelder, J. S.; Van Loosdrecht, M. C. M.; Johns, M. L. Chemical Cleaning of Biofouling in Reverse Osmosis Membranes Evaluated Using Magnetic Resonance Imaging. *J. Membr. Sci.* **2010**, *362*, 202−210.

DOI: 10.1021/acsami.9b20385
ACS Appl. Mater. Interfaces 2020, 12, 963−969